Self-Recovering Triboelectric Nanogenerator as Active Multifunctional Sensors

*Mingyuan Ma, Qingliang Liao, Guangjie Zhang, Zheng Zhang, Qijie Liang, and Yue Zhang**

A novel self-recovering triboelectric nanogenerator (STENG) driven by airflow is designed as active multifunctional sensors. A spring is assembled into the STENG and enables the nanogenerator to have self-recovering characteristic. The maximum output voltage and current of the STENG is about 251 V and 56 μA, respectively, corresponding to an output power of 3.1 mW. The STENG can act as an active multifunctional sensors that includes a humidity sensor, airflow rate sensor, and motion sensor. The STENG-based humidity sensor has a wide detection range of 20%–100%, rapid response time of 18 ms, and recovery time of 80 ms. Besides, the STENG could be utilized in the application of security monitoring. This work expands practical applications of triboelectric nanogenerators as active sensors with advantages of simple fabrication and low cost.

1. Introduction

Recently, the triboelectric nanogenerators (TENGs), which operate based on the coupling of triboelectric effect and electrostatic induction, have attracted great attentions.[1,2] The TENGs have been demonstrated to be a cost-effective and high-efficiency approach for scavenging various mechanical energy, such as wind energy, water energy, motion energy, etc.[3–8] This energy generation technique has also been applied for designing various self-powered sensors to detect motion, chemicals, speed, pressure, etc.[9–14] The periodic contact and separation between two triboelectric surfaces with opposite triboelectric charges can periodically change the induced electric potential difference between two electrodes, which can drive electrons to flow through external loads. Four fundamental operation modes of TENGs have been established to accommodate applications in multifarious mechanical motions, namely, the vertical contact-separation mode, the in-plane sliding mode, the single-electrode mode, and the freestanding triboelectric layer mode.[2] However, in most works, TENGs cannot restore to the original state by itself after being triggered and must be realized under external force or power source, which is energy-wasting and low-efficiency. In addition, realization of rapid relative movement between two triboelectric surfaces is one of the challenges to enhance induced charge flow between two electrodes and increase the output performance. If a TENG can not only be self-recovering but also realize rapid relative movement between two triboelectric surfaces, it can be superior for energy harvesting.

Herein, a novel self-recovering triboelectric nanogenerator (STENG) is proposed and fabricated for the first time. This nanogenerator shows a significantly high output performance driven by airflow. The STENG can be employed to detect multiple signals including humidity, airflow rate, and motion. The STENG-based humidity sensor has a wide detection range, rapid response, and recovery time. This work demonstrates

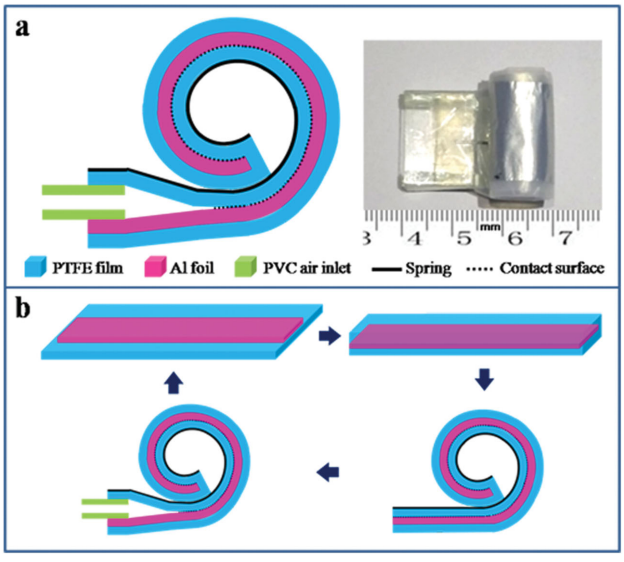

Figure 1. Device structure and fabrication progress of the STENG. a) Schematic diagram of the STENG; the inset is a photograph of the fabricated STENG. b) Fabrication progress of the STENG.

M. Ma, Dr. Q. Liao, G. Zhang, Z. Zhang, Q. Liang, Prof. Y. Zhang
State Key Laboratory for Advanced Metals and Materials
School of Materials Science and Engineering
University of Science and Technology Beijing
Beijing 100083, P.R. China
E-mail: yuezhang@ustb.edu.cn

M. Ma, Dr. Q. Liao, G. Zhang, Z. Zhang, Q. Liang, Prof. Y. Zhang
Key Laboratory of New Energy Materials and Technologies
University of Science and Technology Beijing
Beijing 100083, P.R. China

DOI: 10.1002/adfm.201503180

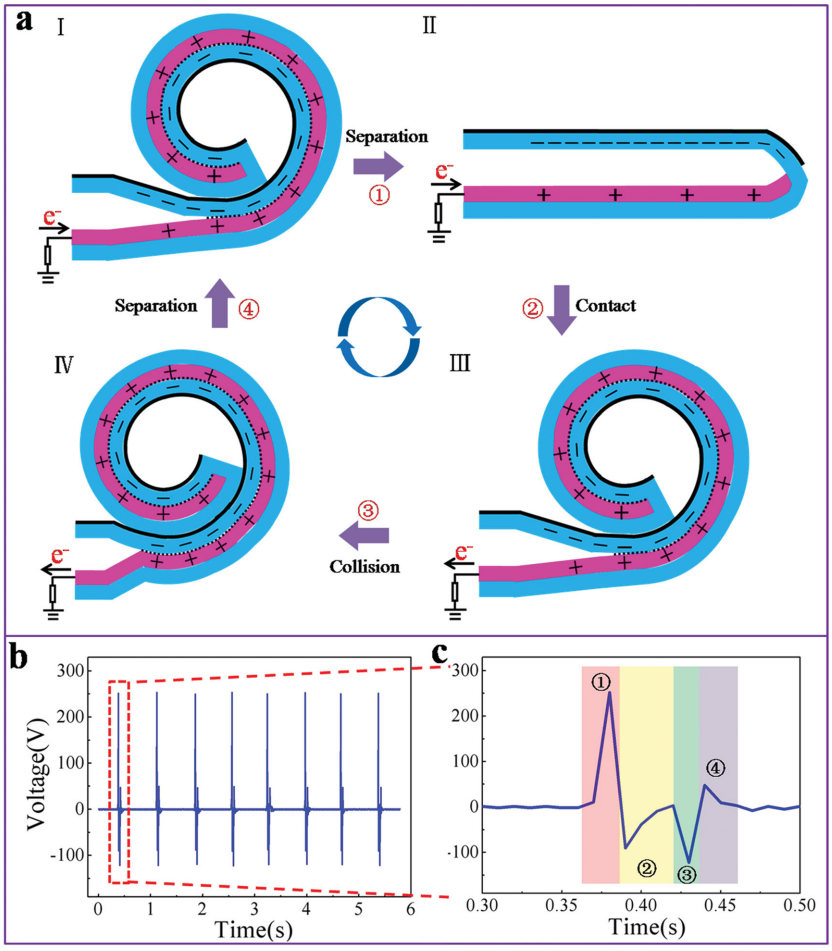

Figure 2. The working mechanism and electrical output performance of the STENG. a) Schematic diagram of the working mechanism of the STENG based on a hybridization of separation-contact-collision-separation progress. b) Output voltage of the STENG. c) Enlarged view of the area indicated by the dashed red box in panel (b).

a novel approach in designing high-performance TENGs and exhibits enormous potential applications of TENG-based sensors.

2. Results and Discussion

The design and fabrication process of the STENG is schematically shown in **Figure 1**. The STENG is composed of an Al foil inside a polytetrafluoroethylene (PTFE) bag, a spring adhered to the PTFE bag, and a polyethylene (PVC) air inlet, as illustrated in Figure 1a. The upper PTFE film acts as a triboelectric surface and the Al foil acts as both the triboelectric surface and the electrode. After triggered by airflow, self-recovering force from the spring can make extremely rapid separation and contact between two triboelectric surfaces.

Figure 2a schematically depicts the working principle of the STENG, which is a hybridization of separation-contact-collision-separation progress. The working mechanism of the STENG depends on the combination of triboelectric effect and electrostatic induction.[1] At original position, the inner surface of the upper PTFE film is in contact with the Al foil. Electrons are injected from the Al foil to the PTFE film since Al is more triboelectrically negative than PTFE due to their different triboelectric polarities,[15] which generates positive triboelectric charges on the Al foil and negative charges on the PTFE film (Figure 2aI). Once air blows through the air inlet, the PTFE bag will swell and the attached spring will stretch up. The two triboelectric surfaces separate from each other and result in the decrease of the induced positive charges on the Al foil, which requires electrons to flow from the ground to the Al electrode (Figure 2aII). Afterward, airflow is stopped and the PTFE bag is rolled acceleratingly by the restoring force from the stretched spring. In response to the increased contact of the Al film and the PTFE film, electrons flow back from the Al electrode to the ground (Figure 2aIII). After the STENG reaches its initial position, it keeps moving up at a high speed owing to the inertia. Thus, the rolled part comes into collision with the inclined part of the STENG, leading to an intense contact between the Al film and the PTFE film and electrons flow from the Al electrode to the ground (Figure 2aIV). Then, the rolled part ceases to move up and rolls back to original position due to the restoring force of the compressed spring and electrons flow back from the ground to the Al electrode (Figure 2aI). At this point, a full cycle of electricity generation progress is completed. With the further blowing of air, another cycle of electricity generation progress similar to the progress from Figure 2aI–aIV will start.

To characterize the performance of the STENG, the electricity output measurement was carried out under helium gas flow by an air gun. Figure 2b shows the output voltage under helium gas flow at a rate of 7.5 L min^{-1}, where the output voltage is extremely high up to 251 V.[3,16–19] The output current and output power of the fabricated STENG is about 56 μA and 3.1 mW on a load of 1 MΩ (Figure S1, Supporting information). The enlarged view of one voltage cycle is shown in Figure 2c. The experimental data validate the electricity generation mechanism described in Figure 2a. First, the two triboelectric surfaces are in contact with each other. When airflow blows in, the triboelectric surfaces start to separate and electrons flow from the ground to the Al electrode to screen the triboelectric charges on Al film (Figure 2aI→aII). When the gas is released, the two films begin to contact due to the restoring force and an induced negative signal is produced (Figure 2aII→aIII). After this, the PTFE film of the inclined part and the Al film come into collision due to the inertia, generating an induced negative signal (Figure 2aIII→aIV). Then the triboelectric surfaces start to separate due to the restoring force, and another induced positive signal is produced (Figure 2aIV→aI).

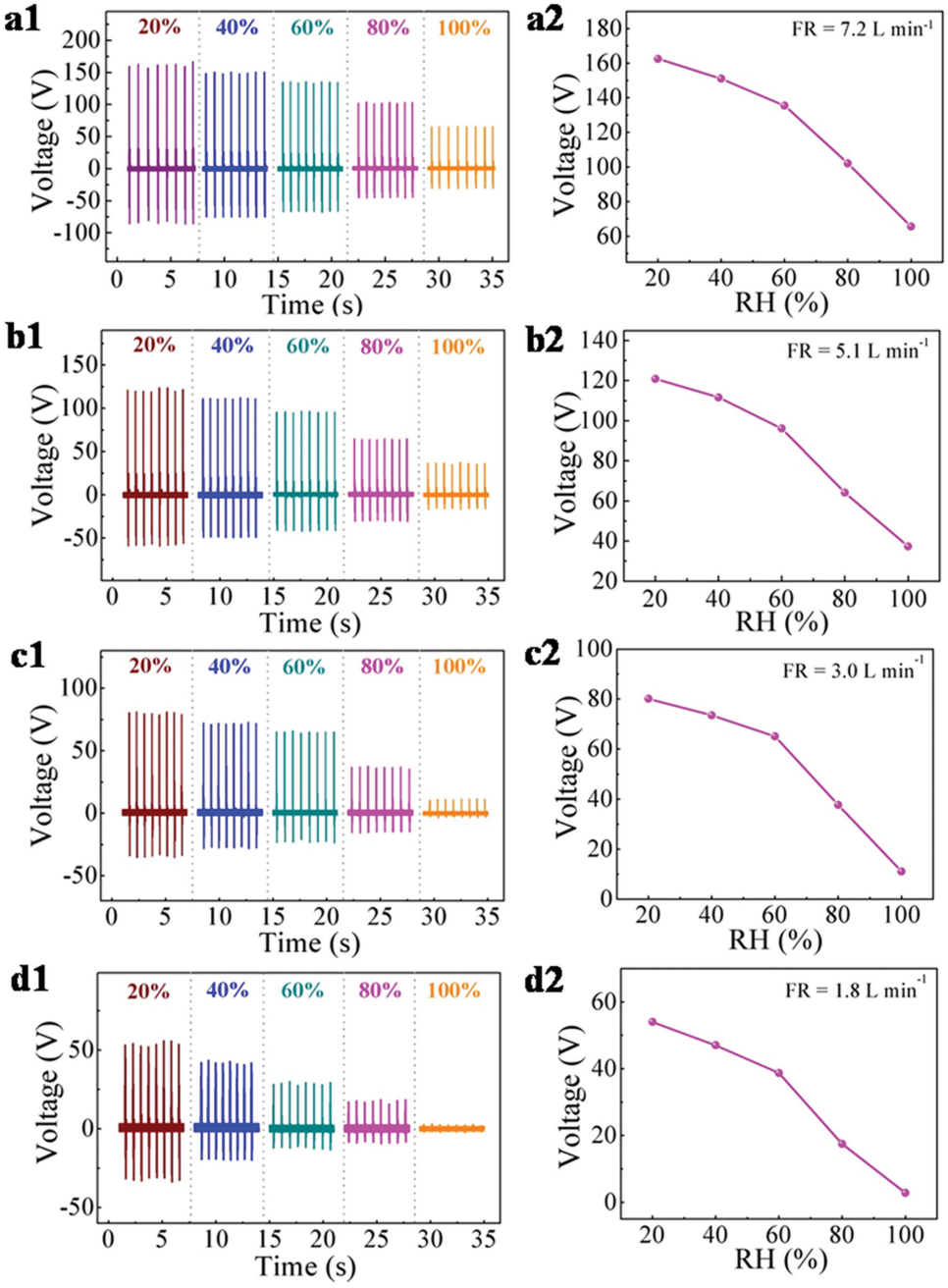

Figure 3. The output voltage of STENGs with varying relative humidity driven by different airflow rates. FR = a1) 7.2, b1) 5.1, c1) 3.0, and d1) 1.8 L min^{-1}. a2–d2) Corresponding spot dates of panels (a1)–(d1).

It is observed that the voltage signal for contact when air blows out has a smaller magnitude but longer duration than that for separation when air blows in. It can be explained by faster separation resulting from external high rate of airflow compared to slower contact caused by the restoring force of the spring.[20–22] Similarly, because the collision resulting from the inertia is faster than separation caused by the restoring force of the spring, the voltage signal for separation has a smaller magnitude but longer duration than that for collision. The output performance of the STENGs under different elastic coefficient of the spring was tested (Figure S2, Supporting Information). It is found that the positive voltage value decreases with an increase in elastic coefficient, but the negative voltage value increases as elastic coefficient increases. The reason for this phenomenon is that larger elastic coefficient causes larger resistance when air blows in, which results in slower separation between the two triboelectric surfaces. While larger elastic coefficient brings larger restoring force when air blows out, which leads to faster contact between the two triboelectric surfaces.

In industrial manufacturing and environmental monitoring, humidity detection is crucial and of great practical value.[23,24] Aimed to demonstrate the STENG can behave a humidity sensor,

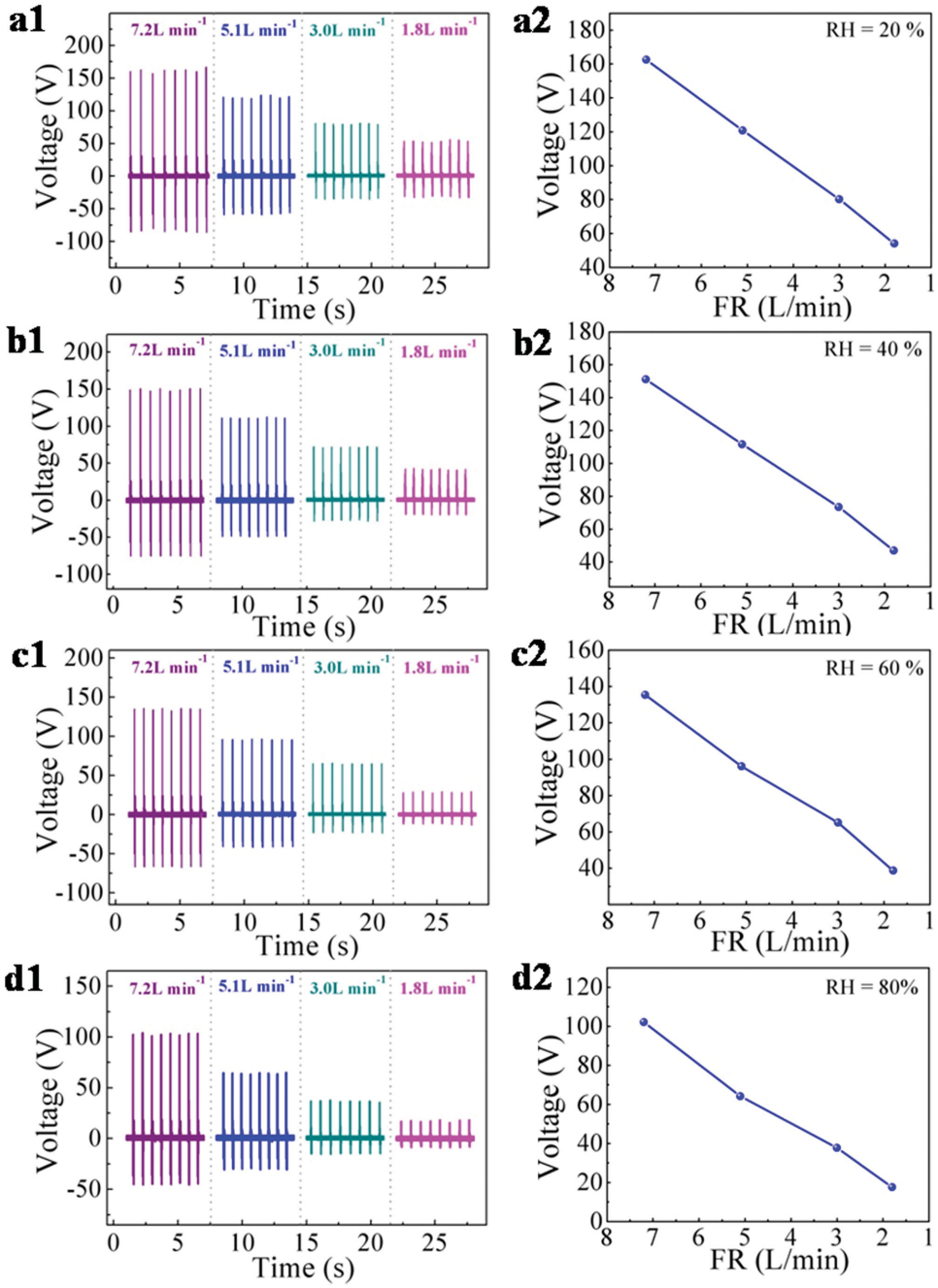

Figure 4. The output voltage of STENGs with changing flow rate under different relative humidity. RH = a1) 20, b1) 40, c1) 60, and d1) 80. a2–d2) Corresponding spot dates of panels (a1)–(d1).

the output performance of the STENG in various humidity conditions was measured, as shown in **Figure 3**. Figure S3 (Supporting information) presents the schematic diagram for the humidity response experiment setup. Figure 3a1–d1 demonstrates the output voltage performance of the STENG in different relative humidity (RH) values (include 20%, 40%, 60%, 80%, and 100%) under the same flow rate (FR) conditions, which indicates that the output voltage decreases with an increase in RH. Figure 3a2–d2 shows the relationship between the output voltage and RH. With RH increasing from 20% to 100%, the output voltage decreases from 162.5 to 65.5 V at 7.2 L min^{-1}, from 120.8 to 37.3 V at 5.1 L min^{-1}, from 80.1 to 11 V at 3.0 L min^{-1}, and from 54 to 2.8 V at 1.8 L min^{-1}. The response time to humidification change from 20% to 100% at 7.2 L min^{-1} is about 18 ms, and the recovery time is about 80 ms, as shown in Figure S4 (Supporting Information). Ultrashort response time and recovery time are due to the rapid airflow and fast self-recovering feature of the STENG. Experimental results suggest that output voltage can be a variable to detect humidity. The reason can be explained that PTFE film and Al foil in humid

environment can absorb water molecules to form a water layer on the surface, which can screen the triboelectric charges generated on the surface and decrease the electrical output of the device.[25,26] The STENG in higher humidity condition is inclined to absorb more water molecule on the surface of PTFE film and Al foil to form a larger water layer, hence output voltage decreases as RH increases. The output voltage decreases as the RH increases gradually, which is consistent with the variation trend of the triboelectrically charged area to RH.

FR has been studied as another key factor to affect the output voltage performance of the STENG.[3,19,27] Based on the data of the humidity sensor, the stability of FR is from 20% RH to 80% RH. **Figure 4** shows the output voltage performance of the STENG driven by different FR (include 7.2, 5.1, 3.0, and 1.8 L min^{-1}) in constant humidity conditions and the plot of the output voltage versus FR. The results indicate that when the FR declines from 7.2 to 1.8 L min^{-1}, the output voltage decreases from 162.5 to 54 V in 20% RH, from 162.5 to 54 V in 20% RH, from 151 to 47 V in 40% RH, from 135.4 to 38.4 V in 60% RH, and from 102.1 to 17.5 V in 80% RH. The fitting line demonstrates that the output voltage almost linearly decreases as the RH decreases, which may be caused by a faster separation between PTFE film and Al foil at a higher FR. The experimental results demonstrate that output voltage can be a variable to detect FR and higher sensitivity could be obtained in lower humidity value.

To systematically analyze the STENG-based sensor response to changing RH and FR, a 3D graph was plotted, as depicted in **Figure 5**. An overall variation trend of output voltage with the change of RH and FR can be simultaneously calculated from the 3D graph. It can be seen that the voltage declines as the RH increases, however, a reverse trend occurs with the variation of the FR. From the above, the STENG is utilized to not only sense humidity but also detect airflow rate.

In order to demonstrate the potential ability of STENG in motion monitoring, a STENG is integrated with an air pump and light emitting diodes (LEDs) to construct a wireless motion monitoring system, as demonstrated in **Figure 6**. The STENG is able to generate a voltage signal when the air pump is pressed by footsteps which can directly light up tens of LEDs connected in series, as shown in Figure 6c,d. As air blows into the STENG through the air inlet when stepped on the air pump, the STENG will begin to swell due to the increase of air input. When the air pump is released, the air will be out and the STENG will be immediately self-recovering. The separation and contact of the two triboelectric surfaces will induce a change in electric potential difference between the Al electrode and the ground, thus the warning LEDs could be triggered. As presented in Figure 6e, larger external force creates faster separation between the two contact films and generates a higher output voltage. The STENG can serve a stable and simple approach to realize motion monitoring compared to conventional techniques. Moreover, the STENG-based wireless system can be applied as a security monitoring system. When somebody steps on the STENG, the warning LEDs will be set off.

3. Conclusion

In summary, a novel type of STENG has been fabricated and demonstrated as active multifunctional sensors. The STENG produces a maximum output voltage of 251 V and output current of 56 μA with an output power of 3.1 mW. The device was applied as multifunctional sensors to detect humidity, airflow rate, and motion. The detection range of the STENG-based humidity sensor is from 20% to 100%. The response and

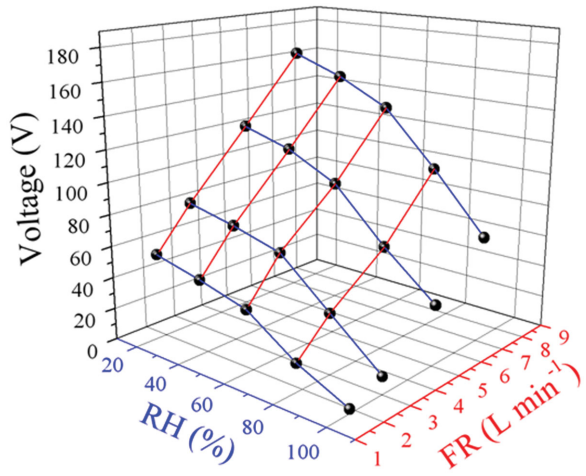

Figure 5. 3D graph of the STENG sensor response to the changing external RH and FR.

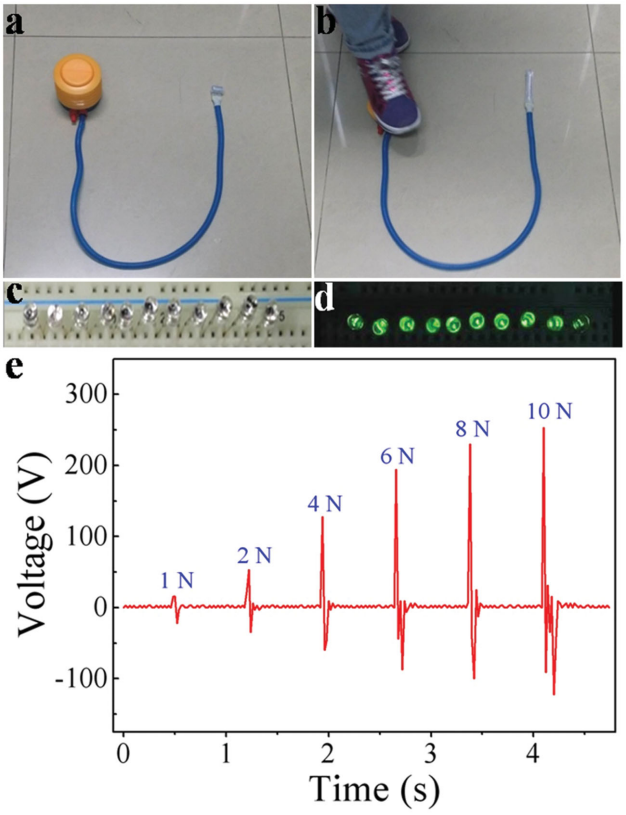

Figure 6. The STENG applied in motion monitoring. a) Photograph of a wireless motion monitoring system. b) Photograph of LEDs driven by a footstep on the air pump. c) Photograph of the original LEDs before being driven. d) Photograph of the LEDs was lighted when stepped on the air pump. e) Output voltage responses to external force.

recovery time are 18 ms and 80 ms, respectively. Furthermore, the STENG can be applied in the field of security monitoring. This work proposes new approaches to design TENGs and indicates great potential of TENGs as multifunctional sensors.

4. Experimental Section

Fabrication of the STENG: A rectangular (4.5 cm × 6 cm) PTFE film with a thickness of 30 μm was prepared as a substrate. A 60 μm thick Al foil with a size of 2 cm × 6 cm was securely adhered to the middle of the substrate. Then, the margins of PTFE film were both folded toward the center and packaged together to form a PTFE bag. Subsequently, a spring was anchored on the middle of the upper surface of the PTFE bag and then the device would be rolled with the inner surface of PTFE bag and the Al foil contacting with each other intimately. Finally, a PVC air inlet with a size of 0.6 cm × 2 cm × 1.5 cm was connected to the end of the bag to form an air-blowing channel.

Characterization and Electrical Measurement: For the measurement of electrical outputs of the STENG, a digital oscilloscope (RIGOL DS4052) with 100 MΩ probe and a Stanford low-noise current preamplifier (Model SR570) were used. In order to simulate an ambient environment with different relative humidity, a glovebox, a humidifier, and a hygrometer were integrated to produce various humidity conditions. A mechanical pump was used to generate airflow and connected with a rotameter to confirm the flow rate.

Supporting Information

Supporting Information is available from the Wiley Online Library or from the author.

Acknowledgements

M.M. and Q.L. contributed equally to this work. This work was supported by the National Major Research Program of China (No. 2013CB932601), the Major Project of International Cooperation and Exchanges (No. 2012DFA50990), the Program of Introducing Talents of Discipline to Universities (B14003), National Natural Science Foundation of China (Nos. 51172022, 51232001, 51372020, and 51527802), the Fundamental Research Funds for Central Universities, State Key Lab of Advanced Metals and Materials (2014Z-11), and Program for New Century Excellent Talents in Universities (NCET-12-0777).

Received: July 31, 2015
Revised: August 23, 2015
Published online: September 23, 2015

[1] Z. L. Wang, *ACS Nano* **2013**, *7*, 9533.
[2] Z. L. Wang, *Faraday Discuss.* **2014**, *176*, 447.
[3] Y. Yang, G. Zhu, H. L. Zhang, J. Chen, X. D. Zhong, Z.-H. Lin, Y. J. Su, P. Bai, X. N. Wen, Z. L. Wang, *ACS Nano* **2013**, *7*, 9461.
[4] Q. J. Liang, X. Q. Yan, Y. S. Gu, K. Zhang, M. Y. Liang, S. N. Lu, X. Zheng, Y. Zhang, *Sci. Rep.* **2015**, *5*, 9080.
[5] F. Yi, L. Lin, S. M. Niu, P. K. Yang, Z. N. Wang, J. Chen, Y. S. Zhou, Y. L. Zi, J. Wang, Q. L. Liao, Y. Zhang, Z. L. Wang, *Adv. Funct. Mater.* **2015**, *25*, 3688.
[6] L. Zheng, Z. H. Lin, G. Cheng, W. Z. Wu, X. N. Wen, S. M. Lee, Z. L. Wang, *Nano Energy* **2014**, *9*, 291.
[7] F. Yi, L. Lin, S. M. Niu, J. Yang, W. Z. Wu, S. H. Wang, Q. L. Liao, Y. Zhang, Z. L. Wang, *Adv. Funct. Mater.* **2014**, *24*, 7488.
[8] W. Q. Yang, J. Chen, G. Zhu, J. Yang, P. Bai, Y. J. Su, Q. S. Jing, X. Cao, Z. L. Wang, *ACS Nano* **2013**, *7*, 11317.
[9] Q. J. Liang, Z. Zhang, X. Q. Yan, Y. S. Gu, Y. L. Zhao, G. J. Zhang, S. N. Lu, Q. L. Liao, Y. Zhang, *Nano Energy* **2015**, *14*, 209.
[10] S. H. Wang, L. Lin, Z. L. Wang, *Nano Energy* **2015**, *11*, 436.
[11] Z.-H. Lin, G. Cheng, Y. Yang, Y. S. Zhou, S. Lee, Z. L. Wang, *Adv. Funct. Mater.* **2014**, *24*, 2810.
[12] S. Jung, J. Lee, T. Hyeon, M. Lee, D.-H. Kim, *Adv. Mater.* **2014**, *26*, 6329.
[13] Y. Wu, Q. S. Jing, J. Chen, P. Bai, J. J. Bai, G. Zhu, Y. J. Su, Z. L. Wang, *Adv. Funct. Mater.* **2015**, *25*, 2166.
[14] X. Y. Wei, G. Zhu, Z. L. Wang, *Nano Energy* **2014**, *10*, 83.
[15] A. F. Diaz, R. M. Felix-Navarro, *J. Electrostat.* **2004**, *62*, 277.
[16] Y. N. Xie, S. H. Wang, L. Lin, Q. S. Jing, Z.-H. Lin, S. M. Niu, Z. Y. Wu, Z. L. Wang, *ACS Nano* **2013**, *7*, 7119.
[17] J. Bae, J. Lee, S. Kim, J. Ha, B. S. Lee, Y. Park, C. Choong, J. B. Kim, Z. L. Wang, *Nat. Commun.* **2014**, *5*, 4929.
[18] P. Bai, G. Zhu, Q. S. Jing, J. Yang, J. Chen, Y. J. Su, J. S. Ma, G. Zhang, Z. L. Wang, *Adv. Funct. Mater.* **2014**, *24*, 5807.
[19] S. H. Wang, X. J. Mu, Y. Yang, C. L. Sun, A. Y. Gu, Z. L. Wang, *Adv. Mater.* **2015**, *27*, 240.
[20] G. Zhu, Z.-H. Lin, Q. S. Jing, P. Bai, C. F. Pan, Y. Yang, Y. S. Zhou, Z. L. Wang, *Nano Lett.* **2013**, *13*, 847.
[21] Y. F. Hu, J. Yang, Q. S. Jing, S. M. Niu, W. Z. Wu, Z. L. Wang, *ACS Nano* **2013**, *7*, 10424.
[22] J. Chen, G. Zhu, W. Q. Yang, Q. S. Jing, P. Bai, Y. Yang, T.-C. Hou, Z. L. Wang, *Adv. Mater.* **2013**, *25*, 6094.
[23] N. Yamazoe, Y. Shimizu, *Sens. Actuators* **1986**, *10*, 379.
[24] Z. Chen, C. Lu, *Sens. Lett.* **2005**, *3*, 274.
[25] H. L. Zhang, Y. Yang, Y. J. Su, J. Chen, C. G. Hu, Z. K. Wu, Y. Liu, C. P. Wong, Y. Bando, Z. L. Wang, *Nano Energy* **2013**, *2*, 693.
[26] B. A. Kwetkus, K. Sattler, H.-C. Siegmann, *J. Phys. D: Appl. Phys.* **1992**, *25*, 139.
[27] H. Y. Guo, J. Chen, L. Tian, Q. Leng, Y. Xi, C. G. Hu, *ACS Appl. Mater. Interfaces* **2014**, *6*, 17184.